Mon. Not. R. Astron. Soc. **000**, 000–000 (2010) Printed 4 November 2010 (MN LATEX style file v2.2)

Imprints of dynamical dark energy on weak-lensing measurements

Sirichai Chongchitnan,[1] Lindsay King [2,3]
[1] *Oxford Astrophysics, Denys Wilkinson Building, Keble Road, Oxford, OX1 3RH, United Kingdom,*
[2] *Institute of Astronomy, Madingley Road, Cambridge, CB3 OHA, United Kingdom,*
[3] *Kavli Institute for Cosmology, Madingley Road, Cambridge, CB3 OHA, United Kingdom.*

arXiv:0910.1539v2 [astro-ph.CO] 3 Nov 2010

October 2009

ABSTRACT
We show that simple models of scalar-field dark energy leave a generic enhancement in the weak-lensing power spectrum when compared to the ΛCDM prediction. In particular, we calculate the linear-scale enhancement in the convergence (or cosmic-shear) power spectrum for two best-fit models of scalar-field dark energy, namely, the Ratra-Peebles and SUGRA-type quintessence. Our calculations are based on linear perturbation theory, using gauge-invariant variables with carefully defined adiabatic initial conditions. We find that geometric effects enhance the lensing power spectrum on a broad range of scales, whilst the clustering of dark energy gives rise to additional power on large scales. The dark-energy power spectrum for these models are also explicitly obtained. On degree scales, the total enhancement may be as large as 30-40% for sources at redshift ~ 1. We argue that there are realistic prospects for detecting such an enhancement using the next generation of large telescopes.

Key words: cosmology – dark energy – gravitational lensing.

1 INTRODUCTION

Over the past years, a concordance picture of our universe has emerged from a number of cosmological probes. In this paradigm, the dominant form of matter is cold and dark (CDM), but most of the mass-energy budget is in the form of dark energy, manifest in the accelerated expansion of the universe [for some of the earliest evidence from Type Ia supernovae, see for example Goldhaber & Perlmutter (1998) and Riess et al. (1998)]. Some of the key goals in cosmology from the analysis of upcoming high-precision experiments within the next couple of decades are to determine the nature of dark energy, and whether there is a tension with its interpretation as a cosmological constant.

A decisive way to distinguish whether dark energy is the cosmological constant or some other dynamical entity is to establish whether the dark-energy equation-of-state parameter $w_{\rm DE}$ is constant or varies with redshift. The variation of $w_{\rm DE}$ can be probed via a range of astronomical techniques, including measurements of light-curves of type Ia supernova (SNIa), cosmic microwave background (CMB) anisotropies, galaxy redshift surveys, galaxy cluster abundance and cosmological weak lensing (see Copeland et al. (2006); Frieman et al. (2008) for a summary of the various techniques).

Out of these techniques, weak lensing holds great promise in the understanding of dark energy, and has been identified as the most powerful individual technique, or most important component in a multi-technique study, provided systematic errors are well understood (Albrecht et al. 2006; Peacock et al. 2006). Its utility as a dark-energy probe comes from sensitivity to both the expansion history of the universe and to the rate of growth of structures.

Observation of weak lensing is still in its infancy, with the first detection of cosmic shear made only nine years ago (Wittman et al. 2000). At present, there are a number of upcoming ambitious experiments - both terrestrial [*e.g.* LSST, ELT (Tyson 2002; Gilmozzi & Spyromilio 2007)] and space-based [*e.g.* JDEM[1], Euclid[2]], aimed at measuring cosmic shear to high accuracy. Given this rapid development, it is worth investigating if the upcoming weak-lensing experiments could discriminate simple models of dynamical dark energy from the cosmological constant.

Many previous works on this problem concentrate solely on the geometrical effects of dynamical dark energy. Furthermore, many authors assume dynamical dark energy with $w_{\rm DE}=$ constant, or some algebraic expression [numerous examples may be found the review by Copeland et al. (2006)]. Whilst this is a useful approximation for studying cosmological dynamics at late-time, it is impossible to extrapolate these simple forms of $w_{\rm DE}$ to early times, unless some *ad hoc* mechanisms are invoked. As a result, one cannot consis-

[1] http://jdem.gsfc.nasa.gov
[2] http://sci.esa.int/euclid

tently analyse the perturbations in dark energy, and many authors then neglect these perturbations altogether. Even those who do include dark-energy perturbations often gloss over the issue of initial conditions, and simply assume that the perturbations are insensitive to initial conditions without any justification.

In this work, we shall calculate the effects of dynamical dark energy on weak-lensing measurements without making any of the assumptions in the previous paragraph. We shall analyse simple models of dynamical dark energy using gauge-invariant perturbation theory, with well-defined initial conditions. As we shall see, these models leave some interesting imprints on the weak-lensing observables on all scales. Ultimately, we shall give a basic assessment of the prospects for distinguishing dynamical dark energy from the cosmological constant using weak-lensing measurements.

One particularly important aspect of this work is the inclusion of dark-energy perturbations throughout our analysis. There have been a number of recent works examining the effects of dark-energy perturbations on cosmological observables (Dent et al. 2008; Sapone & Kunz 2009; Hwang et al. 2009), including some interesting numerical simulations (Alimi et al. 2009; Jennings et al. 2009). Our approach is complementary to these works, and goes further in quantitatively establishing the effects of dynamical dark energy on weak-lensing power spectra. As a by-product, we obtain explicitly, for the first time, the dark-energy power spectrum for these models. Such a spectrum is useful as it quantifies the clustering of dark energy as a function of physical length scale.

Throughout this paper, we work in Planck units in which $c = \hbar = 1$.

2 DYNAMICAL DARK ENERGY

One of the simplest and most widely studied models of dynamical dark energy is *quintessence* - a scalar field evolving slowly along a potential $V(\phi)$ (Caldwell et al. 1998; Ratra & Peebles 1988; Wetterich 1988; Ferreira & Joyce 1998). In this work, we shall focus on the weak-lensing signatures of two particular models of quintessence, namely, the Ratra-Peebles and the SUGRA models.

2.1 The Ratra-Peebles potential

The inverse power-law potential of the form

$$V(\phi) = \frac{M^{4+\alpha}}{\phi^\alpha}, \quad \alpha > 0 \tag{1}$$

has been investigated by Ratra & Peebles (1988) and Wetterich (1988). In this model, the dark-energy density tracks the background energy density by mimicking the equation of state during radiation and matter epochs, and subsequently dominates only at late times. This tracking behaviour holds generally for a wide range of initial conditions.

The attractor properties depend on the slope α roughly as follows. When α is large, the potential becomes very flat for large values of ϕ, hence effectively mimicking the cosmological constant at late times. However, the steep part of the potential for small values of ϕ tends to induce a prolonged matter-dominated epoch. Constraints from distance measurements tend to favour smaller values of α, although the initial conditions then become increasingly difficult to adjust (note that the quintessence would require as much fine-tuning as the cosmological constant as $\alpha \to 0$). A trade-off therefore has to be made in this respect. Given the slope, the self-coupling constant M can then be set to match the value of the dark energy density today. Typically $M \ll m_{\rm pl}$ and therefore there is inevitably a hierarchy problem associated with such a light scalar field. We do not concern ourselves with this issue here, but refer the reader to discussions elsewhere (Carroll 1998; Frieman et al. 1995).

In this paper, we set the self-coupling constant $M = 4.9$ eV and the slope $\alpha = 0.5$, given by Alimi et al. (2009), who obtained these 'best-fit' values from a likelihood analysis of the WMAP 5-year data (Komatsu et al. 2009) and the 'union' SNeIa data (Kowalski et al. 2008) [see also earlier studies by (Klypin et al. 2003; Solevi et al. 2006; Dolag et al. 2004; Maio et al. 2006; Casarini et al. 2009) who investigated slightly different values of the parameters].

2.2 The 'SUGRA' potential

This potential is of the Ratra-Peebles form augmented by an exponential term:

$$V(\phi) = \frac{M^{4+\alpha}}{\phi^\alpha} e^{4\pi G\phi^2}. \tag{2}$$

Brax & Martin (1999) obtained this potential based on the motivation that a supersymmetric correction should be incorporated into the quintessence potential as ϕ can attain a large value exceeding a Planck mass at late times. With this correction, the dynamical behaviour is now less sensitive to the value of α, which is loosely constrained to be of of order 1, and the scalar field need not be as light as the Ratra-Peebles case. Again we shall use the values of the constants based on the analysis of Alimi *et al.*, namely $\alpha = 1$ and $M = 2.1 \times 10^3$ eV (see also the references cited above).

3 PERTURBATIONS

3.1 Background

We consider a background of a homogeneous, isotropic and spatially flat universe, which can be described by the Friedmann-Robertson-Walker metric

$$ds^2 = -dt^2 + a^2(t) dx^i dx_i,$$

where $a(t)$ is the scale factor given in terms of cosmic time t. We assume that the universe contains only radiation, cold dark matter and dark energy, whilst baryons are neglected throughout. Baryons can alter the clustering of matter via baryonic cooling in dark matter halos (White 2004; Rudd et al. 2008). This, however, only translates to small changes in the the weak-lensing spectra on scales very much smaller than those considered here. As for the geometric effect of quintessence on baryon acoustic oscillations, there are various degeneracies to overcome and preliminary results from N-body simulations do not appear optimistic (Jennings et al. 2010a). For these reasons, we feel that it is reasonable to neglect baryons in this work.

With these assumptions, the Friedmann and acceleration equations relating the Hubble parameter, H, to the energy density, ρ, and pressure, p, are given by

$$H^2 = \frac{\bar{\kappa}^2}{3}\rho = \frac{\bar{\kappa}^2}{3}\left[\rho_m + \rho_r + \rho_\phi\right], \tag{3}$$

$$\dot{H} = -\frac{\bar{\kappa}^2}{2}\left[\rho_m + \frac{4}{3}\rho_r + \rho_\phi + p_\phi\right], \tag{4}$$

where $\bar{\kappa}^2 = 8\pi G$. As a convention, we use the subscripts m, r and ϕ to denote quantities related to dark matter, radiation and dark energy respectively. The 'total' quantities carry no subscript. An overdot indicates a derivative with respect to t unless stated otherwise.

The quintessence field ϕ also satisfies the Klein-Gordon equation

$$\ddot{\phi} + 3H\dot{\phi} + V'(\phi) = 0. \tag{5}$$

The various energy densities obey the conservation equations

$$\dot{\rho}_m + 3H\rho_m = 0, \tag{6}$$

$$\dot{\rho}_r + 4H\rho_r = 0, \tag{7}$$

$$\dot{\rho}_\phi + 3H(\rho_\phi + p_\phi) = 0. \tag{8}$$

The equation-of-state parameter w is defined as the ratio p/ρ. For dark matter and radiation, we have $w_m = 0$ and $w_r = 1/3$ respectively. In the case of the cosmological constant, $w_\Lambda \equiv p_\Lambda/\rho_\lambda = -1$. For quintessence, we have

$$\rho_\phi = \frac{1}{2}\dot{\phi}^2 + V, \qquad p_\phi = \frac{1}{2}\dot{\phi}^2 - V, \qquad w_\phi \equiv \frac{p_\phi}{\rho_\phi}. \tag{9}$$

The effective equation of state is given by

$$w \equiv \frac{p}{\rho} = \frac{\rho_r}{3\rho} + \frac{\rho_\phi}{\rho}w_\phi.$$

In practice, it is more convenient to recast the background evolution equations (4)–(8) in terms of the following dimensionless variables:

$$x \equiv \frac{\bar{\kappa}\dot{\phi}}{\sqrt{6}H}, \qquad y \equiv \frac{\bar{\kappa}}{H}\sqrt{\frac{V}{3}},$$

$$z \equiv \frac{\bar{\kappa}}{H}\sqrt{\frac{\rho_r}{3}}, \qquad u \equiv \frac{\bar{\kappa}}{H}\sqrt{\frac{\rho_m}{3}}, \qquad \lambda \equiv -\frac{1}{\bar{\kappa}V}\frac{dV}{d\phi}.$$

This yields a set of differential equations:

$$\frac{d\ln H}{dN} = -\frac{3}{2}\left(1 + x^2 - y^2 + \frac{z^2}{3}\right),$$

$$\frac{dx}{dN} = \sqrt{\frac{3}{2}}\lambda y^2 - x\left(3 + \frac{d\ln H}{dN}\right),$$

$$\frac{dy}{dN} = -\sqrt{\frac{3}{2}}\lambda xy - y\frac{d\ln H}{dN},$$

$$\frac{dz}{dN} = -z\left(2 + \frac{d\ln H}{dN}\right),$$

$$\frac{du}{dN} = -u\left(\frac{3}{2} + \frac{d\ln H}{dN}\right),$$

where $N = \ln a$. In addition, x, y, z, u satisfy the Friedmann's constraint

$$x^2 + y^2 + z^2 + u^2 = 1. \tag{10}$$

The dimensionless system above is numerically more robust to integrate, and the dynamics in the phase-space (x, y, z, u) can be easily analysed (Copeland et al. 1998).

In our numerical work, the initial values of the background variables $\{x, y, z, u\}$ were chosen in such a way that the energy densities today are in broad agreement with the observed values:

$$\Omega_{\phi,0} \simeq 0.27, \quad \Omega_{r,0} \simeq 8.6 \times 10^{-5}, \quad \Omega_{m,0} = 1 - \Omega_{\phi,0} - \Omega_{r,0},$$

[see *e.g.* Komatsu et al. (2009); Kowalski et al. (2008); Kessler et al. (2009)]. For computational convenience, we shall work with the dimensionless density parameter $\Omega \equiv \rho/\rho_c$ (where the critical density $\rho_c \equiv 3H_0^2/\bar{\kappa}^2$) instead of ρ. The subscript 0 indicates the present-day value.

In terms of Ω, Friedmann's equation (3) becomes the constraint

$$\Omega = \Omega_m + \Omega_r + \Omega_\phi,$$

with $\Omega = 1$ at the present time. The density parameters redshift according to

$$\Omega_m = \Omega_{m,0}\,(1+z)^3, \tag{11}$$

$$\Omega_r = \Omega_{r,0}\,(1+z)^4, \tag{12}$$

$$\Omega_\phi = \Omega_{\phi,0}\,(1+z)^3 \exp\Theta(z), \tag{13}$$

$$\Theta(z) = 3\int_0^z \frac{w_\phi(z')}{1+z'}dz'. \tag{14}$$

3.2 Gauge-invariant variables

Working in Newtonian gauge and neglecting anisotropic stresses, vector and tensor perturbations, the Friedman-Robertson-Walker metric with scalar metric perturbation Φ takes the usual form

$$ds^2 = -(1+2\Phi)dt^2 + a^2(t)(1-2\Phi)dx^i dx_i. \tag{15}$$

The components of the energy-momentum tensor are

$$T_0^0 = -\rho, \quad T_\mu^0 = -\frac{1}{k}(\rho + p)v_{,\mu}, \qquad T_\mu^\nu = p\delta_\mu^\nu, \tag{16}$$

where the total energy density ρ decomposes into the background value $(\bar{\rho}_m + \bar{\rho}_r + \bar{\rho}_\phi)$ and the perturbed part $(\delta\rho_m + \delta\rho_r + \delta\rho_\phi)$ and k is the wavenumber. The total pressure p and velocity v can be similarly decomposed.

We define the density contrasts δ and the quintessence perturbation $\delta\phi$ by

$$\delta_m = \frac{\delta\rho_m}{\bar{\rho}_m}, \quad \delta_r = \frac{\delta\rho_r}{\bar{\rho}_r}, \quad \phi = \bar{\phi} + \delta\phi\,. \tag{17}$$

The total metric perturbation comprises contributions from all three components:

$$\Phi = \Phi_m + \Phi_r + \Phi_\phi, \tag{18}$$

where each component relates to the scalar perturbations via Poisson's equation in Fourier space

$$\Phi_i = \frac{3}{2}\left(\frac{aH_0}{k}\right)^2(\Omega_i\Delta_i)\,, \tag{19}$$

with $i = m, r, \phi$. Here, the gauge-invariant density variables

Δ_i are given by

$$\Delta_m = \delta_m + 3\left(\frac{aH}{k}\right)v_m, \tag{20}$$

$$\Delta_r = \delta_r + 4\left(\frac{aH}{k}\right)v_r, \tag{21}$$

$$\Delta_\phi = \frac{\dot\phi\dot{\delta\phi} + [3H\dot\phi + V'(\phi)]\delta\phi + \dot\phi^2\Phi}{\frac{1}{2}\dot\phi^2 + V(\phi)}, \tag{22}$$

$$v_\phi = \frac{k\,\delta\phi}{a\dot\phi}, \tag{23}$$

(Kodama & Sasaki 1984). Note that in Newtonian gauge, it is Δ, and not δ, that appears in Poisson's equation. The variable Δ is velocity-dependent, but in practice one finds that the velocity effect is only noticeable on the largest scales.

The gauge-invariant variables $\{\Delta_i, v_i\}$ evolve via a set of six coupled differential equations (Kodama & Sasaki 1984):

$$\frac{d\Delta_m}{dz} = \frac{k}{H}v_m - \frac{9}{2}\frac{a^2H}{k}(1+w)(\bar v - v_m), \tag{24}$$

$$\frac{d\Delta_r}{dz} + \frac{\Delta_r}{1+z} = \frac{4k}{3H}v_r - 6\frac{a^2H}{k}(1+w)(\bar v - v_r), \tag{25}$$

$$\frac{d\Delta_\phi}{dz} + \frac{3w_\phi\Delta_\phi}{1+z} = \frac{\dot\phi^2}{\rho_\phi}\left[\frac{k}{H}v_\phi - \frac{9}{2}\frac{a^2H}{k}(1+w)(\bar v - v_\phi)\right], \tag{26}$$

$$\frac{dv_m}{dz} - \frac{v_m}{1+z} = \frac{3a^2H}{2k}\bar\Delta, \tag{27}$$

$$\frac{dv_r}{dz} - \frac{v_r}{1+z} = \frac{3a^2H}{2k}\bar\Delta - \frac{k}{4H}\Delta_r, \tag{28}$$

$$\frac{dv_\phi}{dz} - \frac{v_\phi}{1+z} = \frac{3a^2H}{2k}\bar\Delta - \frac{k}{(1+w_\phi)H}\Delta_\phi, \tag{29}$$

where

$$\bar v = \frac{1}{\rho(1+w)}\left(\dot\phi^2 v_\phi + \frac{4}{3}\rho_r v_r + \rho_m v_m\right), \tag{30}$$

$$\bar\Delta = \frac{1}{\rho}\left(\rho_m\Delta_m + \rho_r\Delta_r + \rho_\phi\Delta_\phi\right). \tag{31}$$

The power spectrum of component i is defined as

$$P_i(k) \equiv \frac{1}{(2\pi)^3}\langle|\Delta_i(k)|^2\rangle. \tag{32}$$

Assuming that the primordial spectrum $P_m(k)$ scales with k^{n_s}, where n_s is the scalar spectral index, it can be shown that

$$P_m(k) = 2\pi^2\delta_H^2\frac{k^{n_s}}{H_0^{n_s+3}}\left[\frac{\Delta_m^+(z=0)}{\Delta_m^+(z=z_i)}\right]^2 \tag{33}$$

where the term in brackets is the ratio of the growing-mode amplitudes of matter perturbations Δ_m^+ at redshift $z=0$ and initial redshift z_i [see, *e.g.* Dodelson (2003)]. The amplitude δ_H specifies the normalization of the matter power spectrum at CMB scales. In particular, Liddle et al. (2006) have computed a fitting function for δ_H using results from WMAP (Spergel et al. 2007). Under the assumption that there is no tensor mode, the fitting formula reads

$$\delta_H(k = 0.05\ \mathrm{Mpc}^{-1}) = 1.927\times10^{-5}\exp[-1.24(1-n_s)]. \tag{34}$$

In our numerical work, we shall use the fitting formula above with $n_s = 0.96$, and set the initial redshift at $z_i = 10^9$.

3.3 Initial conditions

We expect the initial conditions for the perturbations in the various components to be set during inflation, and therefore it is reasonable to impose the adiabatic initial conditions on all perturbations. Adiabaticity specifies that at an initial time t_0, the following quantities vanish:

(A1) $\mathcal{S}_{mr}$, the entropic perturbation between dark matter and radiation,
(A2) $\mathcal{S}_{m\phi}$, the entropic perturbation between dark matter and quintessence,
(A3) $\mathcal{I}$, the intrinsic entropic perturbation of quintessence.

The entropic perturbations above are defined as

$$\mathcal{S}_{mr} \equiv \frac{\delta\rho_m}{\dot\rho_m} - \frac{\delta\rho_r}{\dot\rho_r} = 0, \tag{35}$$

$$\mathcal{S}_{m\phi} \equiv \frac{\delta\rho_m}{\dot\rho_m} - \frac{\delta\rho_\phi}{\dot\rho_\phi} = 0, \tag{36}$$

$$\mathcal{I} \equiv \frac{\delta\rho_\phi}{\dot\rho_\phi} - \frac{\delta p_\phi}{\dot p_\phi} = 0, \tag{37}$$

where the perturbations in dark-energy density and pressure satisfy

$$\delta\rho_\phi = \dot\phi\dot{\delta\phi} - \dot\phi^2\Phi + V'\delta\phi, \tag{38}$$

$$\delta p_\phi = \dot\phi\dot{\delta\phi} - \dot\phi^2\Phi - V'\delta\phi. \tag{39}$$

Note that the adiabaticity between radiation and quintessence, namely

$$\mathcal{S}_{r\phi} \equiv \frac{\delta\rho_r}{\dot\rho_r} - \frac{\delta\rho_\phi}{\dot\rho_\phi} = 0, \tag{40}$$

is automatically satisfied.

In terms of the gauge-invariant variables $\{\Delta_i, v_i\}$, the conditions (A1)-(A3) yield respectively

$$\Delta_m - \frac{3}{4}\Delta_r = 3\left(\frac{aH}{k}\right)(v_m - v_r), \tag{41}$$

$$\Delta_m + 3\left(\frac{aH}{k}\right)^2\bar\Delta - \frac{\rho_\phi}{\dot\phi^2}\Delta_\phi = 3\left(\frac{aH}{k}\right)(v_m - v_\phi), \tag{42}$$

$$3\left(\frac{aH}{k}\right)^2\bar\Delta = \frac{\rho_\phi}{\dot\phi^2}\Delta_\phi. \tag{43}$$

Equation (43) can be further combined with (42) to yield

$$\Delta_m = 3\left(\frac{aH}{k}\right)(v_m - v_\phi). \tag{44}$$

Inserting this into (41) gives

$$\Delta_r = 4\left(\frac{aH}{k}\right)(v_r - v_\phi). \tag{45}$$

One can also easily verify that this equation can be obtained directly from (40).

Once the adiabatic conditions (A1)-(A3) are imposed, there remains the freedom to choose three initial values from the set $\{\Delta_i, v_i\}$. Firstly, the initial value of Δ_m is chosen so that the amplitude of the matter power spectrum is normalised on CMB scales according to equation (34). Next, assuming that the velocity perturbations are initially small compared with the density perturbations, we take $\Delta_r = 4\Delta_m/3$ (suggested by the usual adiabatic condition for matter and radiation). Lastly, we set $v_\phi = 0$ initially,

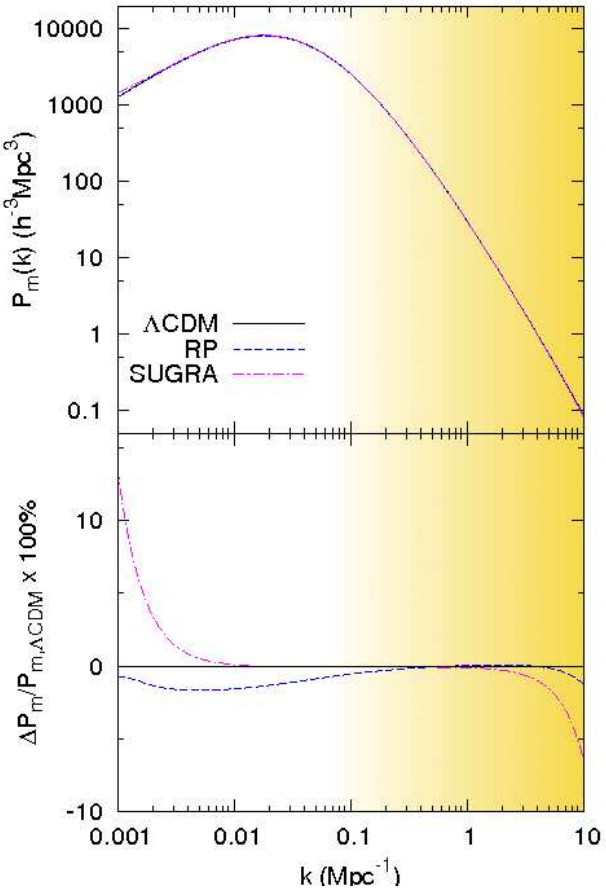

Figure 1. The linear matter power spectra $P_m(k)$ for the case that dark energy is the cosmological constant (solid/black line), the Ratra-Peebles quintessence (dashed/blue) or the SUGRA-type quintessence (dash-dot/magenta). The lower panel shows the fractional difference in $P_m(k)$ expressed as a percentage (equation 46). Non-linear effects manifest in the shaded region starting from $k \sim 0.1$ Mpc^{-1} (though there are other estimates as low as $0.03h$Mpc^{-1}). See text for further discussion.

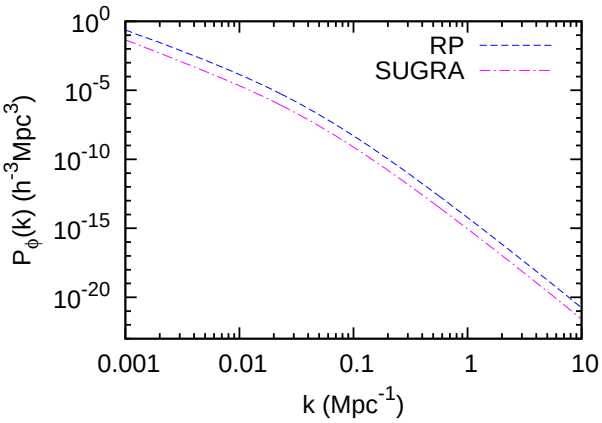

Figure 2. The linear dark-energy power spectra $P_\phi(k)$ for the Ratra-Peebles quintessence and the SUGRA-type quintessence. The spectra are roughly broken into two exponentially decaying regimes, changing around the turnover scale.

as the dark-energy velocity perturbations quickly redshift away and therefore do not have a significant effect the growing mode amplitude. With these choices, all the initial values of $\{\Delta_i, v_i\}$ can be determined by solving the linear system consisting of equations (43),(44) and (45).

It is important to note that adiabaticity implies $\Delta_\phi \neq 0$ initially (*e.g.* from equation 43), and hence dark-energy perturbations cannot be consistently neglected.

3.4 Power spectra

Figure 1 shows the linear matter power spectra $P_m(k)$ for the ΛCDM, Ratra-Peebles and SUGRA models. The lower panel shows the fractional difference in the matter power spectra between the ΛCDM and the quintessence models, expressed as the ratio

$$\frac{P_{\rm m,Quintessence} - P_{\rm m,\Lambda CDM}}{P_{\rm m,\Lambda CDM}} \times 100\%. \qquad (46)$$

The spectra in the upper panel are difficult to distinguish by eye, but the lower panel shows that there are some differences on large scales, where the SUGRA best-fit model yields an excess power of around 10% compared to the ΛCDM model. On the other hand, the Ratra-Peebles best-fit model shows a very slight deviation in power from the ΛCDM case. In both cases, there is a slight suppression in the matter power spectrum on all scales smaller than the turnover scale, corresponding to the Hubble radius at the time of matter-radiation equality. Generally, the differences are inconspicuous, and thus it would be very difficult to distinguish between these models via galaxy redshift surveys and the abundance of massive galaxy clusters.

We also obtained the power spectrum of dark energy $P_\phi(k)$, as shown in figure 2. The amplitudes of these spectra are about 3 orders of magnitude below that of the matter power spectrum, thus showing that the clustering of dark energy is relatively weak. The spectra are roughly broken into two exponentially decaying regimes, changing around the turnover scale (the decay rate is greater for scales smaller than the turnover scale). The clustering power becomes negligible at sufficiently small scales as one might expect. Despite the small amplitude of P_ϕ, the cross-correlation between the matter and the dark energy spectra yield a small but non-negligible contribution to the weak-lensing signal, as we shall see in the next section.

On smaller scales, one expects a significant modification of the various power spectra due to the non-linear evolution of the perturbations. N-body simulations suggest that non-linear effects are important for scales $k \gtrsim \mathcal{O}(0.1$ Mpc$^{-1})$, where corrections are of order $\sim$ 10% (Alimi et al. 2009; Ma et al. 1999; Jennings et al. 2009). (It is worth noting an estimate in Jennings et al. (2010b) which shows non-linearities manifesting on a much larger scale – at around $k \sim 0.03h$Mpc^{-1}.) As far as standard non-linear fitting formulae for matter power spectrum are concerned [*e.g.* Peacock & Dodds (1994); Smith et al. (2003)], they are unreliable in the case when dark energy is dynamical, and they certainly do not shed any light on the non-linear clustering of dark energy. Thus, at present non-linear effects are usually calibrated against N-body simulations. This approach is clearly inefficient as they can only test a specific combination of parameters for a specific potential at a time.

Some authors have turned to semi-analytic approaches to reproduce non-linear effects (Benabed & Bernardeau 2001; Casarini et al. 2009) but these have not yet been tested sufficiently. From our point of view, combining simulations with field-theoretic calculations such as those developed by Crocce & Scoccimarro (2006) or Bernardeau et al. (2002) may be the most sensible approach in dealing with the strongly non-linear regime. These analytic techniques are still being developed and, as far as we are aware, they are not yet applicable to models with dynamical dark energy. It is possible to calculate perturbations in quintessence cosmology analytically in a weakly non-linear regime using higher-order perturbation theory (Hwang 1991; Malik & Wands 2004), but these methods are very tedious and the results would be valid only on a narrow range of non-linear scales. We shall leave the issue of non-linearity for future investigation.

4 WEAK-LENSING SIGNALS

4.1 The convergence spectrum

The weak gravitational lensing of a light source may be quantified by two fields: the convergence κ, and the gravitational shear γ [see Bartelmann & Schneider (2001) for a review]. The convergence magnifies sources isotropically, and is therefore not directly observable unless the size of the source is known *a priori*. In the weak lensing limit, the power spectrum of the convergence can be shown to be equivalent to the power spectrum of the cosmic shear, which is observable as a correlated distortion in the (complex) ellipticities of distant galaxies (ignoring any intrinsic alignment). In this work, we shall focus on the convergence power spectrum, although it can be equivalently replaced by that of the shear.

The convergence associated with a light source at comoving distance r in the direction $\vec{\theta}$, resulting from the cumulative effect of density fluctuations at comoving distance r' is given by

$$\kappa(\vec{\theta},r)=\int_0^r dr'\left(\frac{r-r'}{r}\right)r'\nabla^2\Phi(r'\vec{\theta},r'). \tag{47}$$

By integrating over all sources up to the Hubble radius r_H, the effective convergence in the direction $\vec{\theta}$ is

$$\kappa(\vec{\theta})=\int_0^{r_H} dr\, W(r)\, r\, \nabla^2\Phi(r\vec{\theta},r). \tag{48}$$

Here, the weight function

$$W(r)=\int_r^{r_H} dr' G(r')\left(\frac{r'-r}{r'}\right), \tag{49}$$

contains information on the distribution of sources along the line of sight. The function $G(r)$ is related to the source redshift distribution $p_z(z)$ by $G(r)dr=p_z(z)dz$. In this work, we shall only consider sources at a single redshift, so that the weight function reduces to

$$W(r)=\begin{cases}1-r/r^* & \text{if } 0\le r<r^*,\\ 0 & \text{otherwise,}\end{cases}$$

where r^* is the comoving distance to the source.

The convergence power spectrum can be obtained by following essentially the same the derivation as in Bartelmann & Schneider (2001), but taking care of the dark-energy contribution to the total metric perturbation. The procedure involves using (11)-(14),(19), (48) and applying Limber's equation in Fourier space. We also neglect the contribution from radiation since $\Omega_{r,0}$ is small compared with $\Omega_{m,0}$ and $\Omega_{\phi,0}$. The convergence power spectrum, P_κ, expressed as a function of the multipole number, ℓ, is given by

$$P_\kappa(\ell)\simeq\frac{9H_0^4}{4}\int_{0^+}^{r_H}\frac{W^2(r)}{a^2}\Big[\Omega_{m,0}^2P_m\left(\frac{\ell}{r},r\right)+ 2\Omega_{m,0}\Omega_{\phi,0}\exp(\Theta)\,P_{m\phi}\left(\frac{\ell}{r},r\right)+\Omega_{\phi,0}^2\exp(2\Theta)\,P_\phi\left(\frac{\ell}{r},r\right)\Big]dr, \tag{50}$$

with Θ given by equation (14). By setting $P_\phi=P_{m\phi}=0$, we recover the usual convergence power spectrum of Bartelmann & Schneider.

The power spectra $P_i(k,r)$ in the integrand of (50) are evaluated at scale k for which $k=\ell/r$ and at redshift z calculated from the distance-redshift relation

$$r(z)=\int_0^z\frac{dz'}{H(z')}. \tag{51}$$

The range of integration extends to the comoving horizon $r_H=\lim_{z\to\infty}r(z)$.

4.2 Imprints of dynamical dark energy on the convergence

Figure 3 shows the convergence power spectra for the cases in which dark energy is the cosmological constant, Ratra-Peebles or SUGRA-type quintessence, assuming sources at $z=1$. The upper panel shows $\ell^2P_\kappa(\ell)$, the total convergence power per unit logarithmic-ℓ interval. The lower panel shows the percentage difference in the convergence power for the quintessence models compared with the ΛCDM model. The convergence power spectra for the quintessence models are generally enhanced (by around 20% at $\ell\simeq100$ or $\sim2^\circ$) even though there are relatively little differences in the matter power spectra. The enhancement occurs on all scales and in fact *grows* with ℓ.

There are two main effects which contribute to the enhancement of the convergence power. Firstly, dynamical dark energy modifies the distance-redshift relation in such a way that a source at a fixed redshift lies at a greater comoving distance compared with the ΛCDM case (see figure 4). More intervening energy density therefore gives rise to a higher weak-lensing signal. Secondly, dark-energy perturbations contribute to an additional power via the last two terms in equation 50. The cross- and auto-correlation of dark-energy perturbations together contribute an enhancement of a few percent on large scales ($\ell\lesssim10$), as shown in figure 5. The y-axis is the ratio

$$\frac{P_{\kappa,\text{no DE pert}}-P_\kappa}{P_\kappa}\times100\%, \tag{52}$$

where $P_{\kappa,\text{no DE pert}}$ is the convergence power spectrum calculated without the last two terms in equation 50.

One might ask what would happen to the convergence power spectrum if dark-energy perturbations were neglected *altogether*, *i.e.*, if we were to set $\Delta_\phi=v_\phi\equiv0$. This, however,

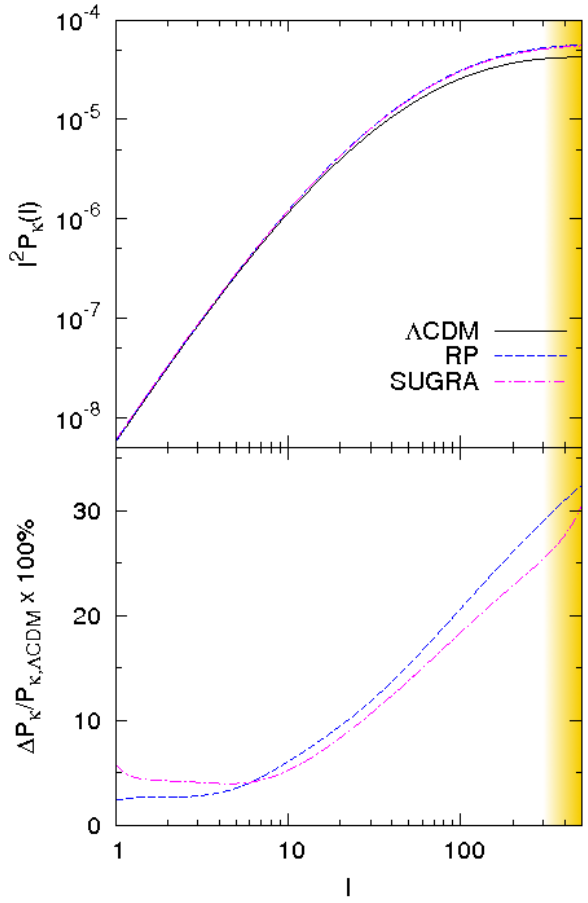

Figure 3. The convergence power per logarithmic ℓ interval for the case that dark energy is the cosmological constant (solid/black line), Ratra-Peebles quintessence (dashed/blue) or the SUGRA-type quintessence (dash-dot/magenta) assuming sources at $z = 1$. The lower panel shows the fractional enhancement in P_κ due to dynamical dark energy, expressed as a percentage. In the shaded region (beyond ℓ of a few hundred), non-linear effects become important. Further discussion is given in the text.

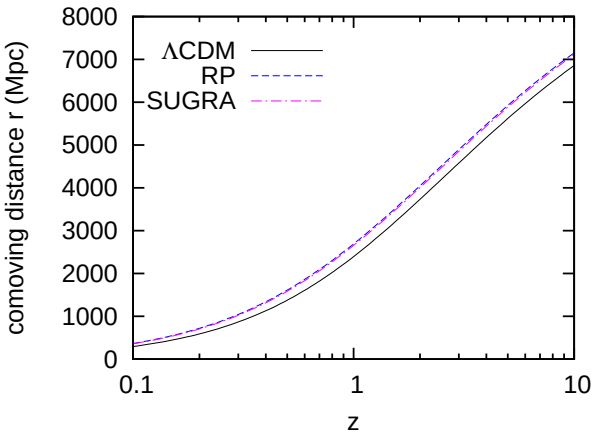

Figure 4. Distance-redshift relations given cosmology in which dark energy is the cosmological constant, Ratra-Peebles or SUGRA-type quintessence. Objects at a fixed redshift are further away in the quintessence cases, partially giving rise to the enhancement seen in figure 3.

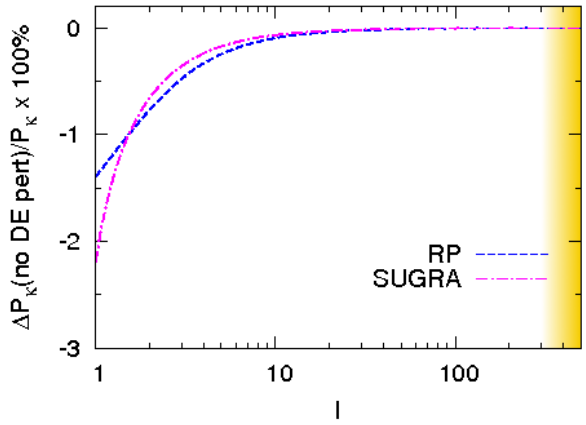

Figure 5. Percentage of error in $P_\kappa(\ell)$ if dark-energy perturbations were not included in the Newtonian potential Φ (*i.e.*, ignoring the last two terms in equation 50). Non-linear region is shaded as in figure 3.

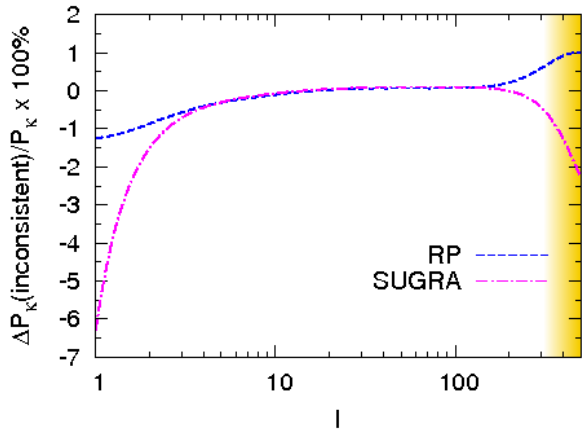

Figure 6. Percentage error in $P_\kappa(\ell)$ if dynamical dark energy were treated as though it does not cluster. The inconsistency is manifest in the divergence on small scales. Non-linear region is shaded as in figure 3.

is an ill-posed problem as all dynamical models of dark energy must cluster, unless $w \equiv -1$ at all times. Neglecting this clustering gives rise to inconsistencies in the evolution equations, and the results will be sensitive to the gauge choice (Hwang et al. 2009). In figure 6, we plot the percentage 'error'

$$\frac{P_{\kappa,\,\text{inconsistent}} - P_\kappa}{P_\kappa} \times 100\%. \qquad (53)$$

The figure shows that the error from ignoring dark energy clustering are of order $\lesssim 10\%$, and can even grow at small scales. Nevertheless, this result is gauge-dependent, and therefore one must refrain from drawing any physical interpretation from this figure. It only serves as a cautionary example against ignoring the clustering of dark energy in the calculation of perturbations.

On smaller scales, we expect an additional enhancement due to non-linear effects, coming solely from the change in geometry since dark energy does not cluster on such small scales. In the ΛCDM model, it is estimated

that linear lensing spectra become unreliable with error $\sim$ 10% on scales beyond $\ell \sim$ few $\times$ 100 (Jain & Seljak 1997; Bartelmann & Schneider 2001), and similarly for models with constant $w_{\rm DE}$ (Huterer 2002; Refregier et al. 2004). This is the reason that we only display our weak-lensing spectra up to $\ell = 500$. Non-linear lensing spectra would certainly be a powerful method of distinguishing between models of dark energy, but as far quintessence are concerned, the non-linear lensing spectra has yet to be understood quantitatively. It would be interesting, though challenging, to investigate this problem using one of the methods described in section 3.4. Our present work nevertheless offers a first step towards understanding the signature of scalar-field dark energy on the weak-lensing spectra.

5 OBSERVATIONAL PROSPECTS

We now consider if an enhanced weak-lensing signal due to dynamical dark energy is potentially observable by future weak-lensing surveys.

The error on the convergence power spectrum arising from cosmic variance and from the intrinsic dispersion in the ellipticities of the galaxies (from which the cosmic shear signal is measured) was derived by Kaiser (1998):

$$\Delta P_\kappa(\ell) = \sqrt{\frac{2}{(2\ell+1)f_{\rm sky}}}\left(P_\kappa(\ell) + \frac{\langle\gamma_{\rm int}^2\rangle}{\bar{n}}\right). \qquad (54)$$

Here f_{sky} is the fraction of the sky covered by a survey of area $\mathcal{A}$ (i.e. $\pi\mathcal{A}/129,600\text{deg}^2$), the mean-square intrinsic ellipticity is $\langle\gamma_{\rm int}^2\rangle \approx 0.16$ and the number of galaxies per steradian for which an ellipticity can be measured is $\bar{n}$.

We consider two specific configurations: (A) $\mathcal{A} = 20,000\,\text{deg}^2$ and a galaxy number density of $250\,\text{arcmin}^{-2}$ and (B) $\mathcal{A} = 30,000\,\text{deg}^2$ and a galaxy number density of $500\,\text{arcmin}^{-2}$. Both configurations require deep imaging using one (A) or more (B) large ground-based telescopes such as the planned European Extremely Large Telescope (E-ELT) (Gilmozzi & Spyromilio 2007), or using future space-based telescopes.

Figure 7 shows the errors (54) associated with these configurations [the outer contour corresponding to configuration (A)], for sources at redshift 1 (top panel) and 0.5 (bottom panel). For sources at $z = 1$, the dark energy enhancement is obscured by the error in measurement below $\ell \simeq 100$, and thus one must look for such a signal at smaller scales. For sources at $z = 0.5$, the prospects are better, with dark-energy enhancement of around 40% at $\ell \simeq 100$, where the errors are minimum.

It is interesting to investigate at what redshift would the best prospects for detection of the dark-energy enhancement be. Figure 8 shows the convergence power at $\ell = 100$ for sources at varying redshifts ($0.1 \lesssim z \lesssim 10$). The upper panel shows a clear upward trend for all three dark energy models. The percentage of deviation from the ΛCDM model is plotted in the lower panel, which shows an interesting tendency for sources at a *lower* redshift to give a higher deviation (at a fixed multipole). By increasing the source redshift, the deviation diminishes and can even disappear altogether (at $z \sim 3$ in this case). Beyond this redshift, the weak-lensing signal at scale $\sim 2^\circ$ is in fact suppressed compared to the ΛCDM case.

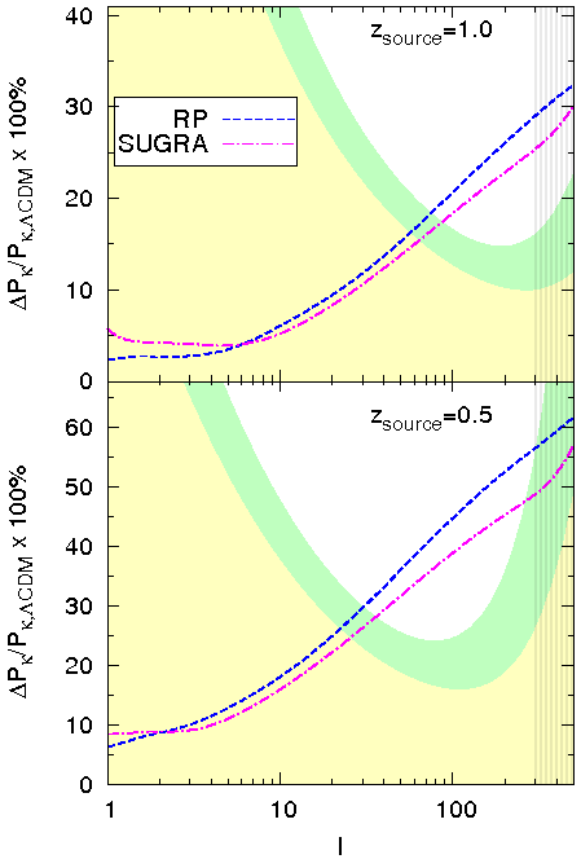

Figure 7. Percentage enhancement in the convergence power for the Ratra-Peebles and SUGRA quintessence, compared with that in the ΛCDM case. The error contours are calculated using equation 54, with (A) $\mathcal{A} = 20,000$ deg^2, galaxy number density = $250\,\text{arcmin}^{-2}$ (outer contour) and (B) $\mathcal{A} = 30,000$ deg^2, galaxy number density = $500\,\text{arcmin}^{-2}$ (inner contour). The sources are at $z = 1$ (top panel) and at 0.5 (bottom panel). Portions of the curves which lie above the shaded contours represent a potentially detectable enhancement. Note that non-linear effects become increasingly important for $\ell \gtrsim$ few $\times$ 100 (grey, striped region), as discussed in the text.

At first sight the suppression of weak-lensing signal for high-redshift sources appears to be in conflict with figure 4, which shows that high-redshift objects are further away in the quintessence scenarios, therefore should enhance the weak-lensing signal due to the fact that there is more intervening energy density. However, recall that in equation 50, the various density power spectra $P(\ell/r, r)$ are smaller at larger r. For sources at a sufficiently large redshift, the weight function becomes more spread out, thus taking into account more contributions from $P(\ell/r, r)$ at large r. This explains the decreasing curves seen in figure 8. Upon imposing the error contours for the same specifications as in figure 7, we see a 'sweet spot' appearing at around $z \simeq 0.5$ where the enhancement level exceeds the intrinsic error by a wide margin. Although this only holds for a single source redshift, we expect our results to be qualitatively correct given a realistic source distribution.

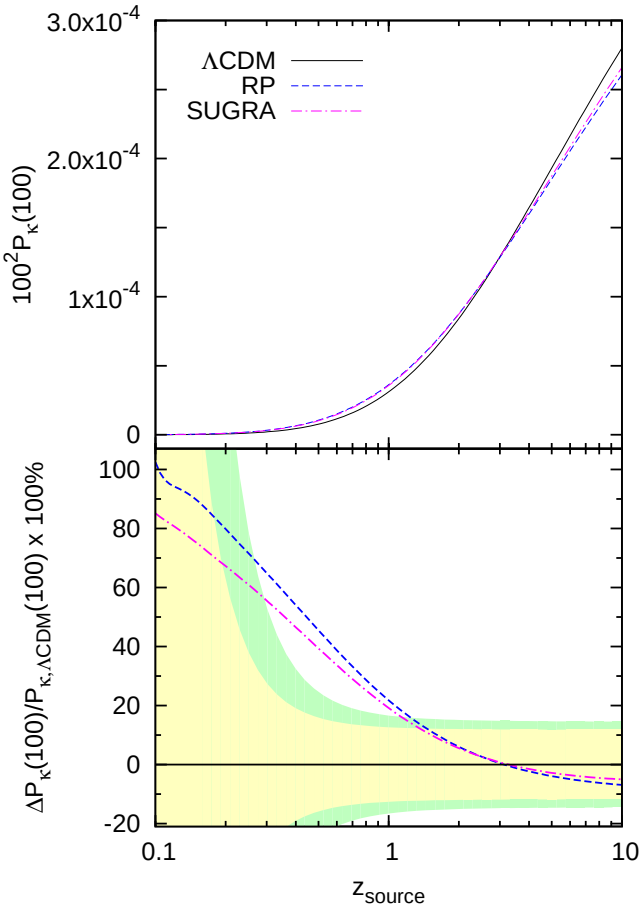

Figure 8. The convergence power at $\ell = 100(\sim 2^\circ)$ as a function of source redshift $z_{\rm source}$. The lower panel shows the fractional difference in $P_\kappa(100)$ expressed as a percentage. The outer (inner) contour corresponds to uncertainty (54) with galaxy number density $= 250\ (500)\,{\rm arcmin}^{-2}$, $\mathcal{A} = 20,000\ (30,000)\,{\rm deg}^2$

In summary, it is possible to distinguish simple models of dynamical dark energy from the cosmological constant via the boost in the weak-lensing power spectra across linear scales. However, the error contours suggest that it would take a network of at least 30-m class telescopes dedicated to cosmic-shear measurement across a large fraction of the sky to detect the dark-energy enhancement, which can be easily obscured at both high and low ℓ by cosmic variance and shot noise. More realistically, there will be additional errors from photometry, systematics in the measurement of galaxy ellipticities, and uncertainties associated with other cosmological parameters. Nevertheless, we expect that they will be subdominant in comparison with the errors calculated in this section.

6 CONCLUSIONS AND DISCUSSIONS

In this work, we have investigated whether there are observable signatures of dynamical dark energy in weak-lensing measurements. Our basic assumptions are that the background cosmology is a flat FRW universe, containing radiation, dark matter and the simplest type of scalar-field dark energy (with no hot dark matter, baryons or tensor modes). Our technique involves calculating the linear density power spectra by integrating six coupled differential equations, expressed in terms of gauge-invariant density and velocity variables for dark matter, radiation and dark energy (equations 24-29). We assume adiabatic initial conditions for all three types of perturbations, and normalise the matter power spectrum (with primordial form $\sim k^{n_s}$) on CMB scales. We base our analysis specifically on two simple models of quintessence, namely the Ratra-Peebles and SUGRA-type potentials, with model parameters that best fit the recent CMB and combined supernova data.

We find that the best-fit quintessence models yield matter power spectra that are hardly distinguishable from that of the ΛCDM model (figure 1) except on large scales where dark-energy clustering is strongest, as shown in figure 2. We believe this is the first time that the dark-energy power spectra for these oft-cited models are explicitly calculated.

When the weak-lensing signals are extracted from the 3D spectra, we found an imprint in the form of an all-scale enhancement in the convergence (or the cosmic shear) power spectrum compared with ΛCDM cosmology. For sources at redshift 0.5, for instance, the enhancement may be as large as 40% at about 2° scale (or 20% at $z = 1$). These enhancements can be attributed to two main reasons, namely i) the change in distance-redshift relation (figure 4), and ii) the lensing by large-scale dark-energy clusters (figure 5).

Assuming that the primary sources of errors in the weak-lensing measurements will be from cosmic variance and intrinsic ellipticity dispersion in the shapes of distant galaxies, there are good prospects for detecting this enhancement for sources at redshift $z \sim 0.5$ using future facilities with surveys covering most of the sky, and capable of measuring ellipticities for hundreds of galaxies per arcmin^2 (figure 7). On the timescale of a decade, one class of telescope capable of such a survey is the E-ELT, 42m in diameter and including adaptive optics, for which operations are planned to start in 2018. To put this requirement in context, current ground-based surveys typically measure ellipticities for a few tens of galaxies per arcmin^2 over order 100 square degrees (e.g. CFHTLS-Wide[3]), and the highest specification near-future survey DES[4] will measure a comparable number density of galaxies over 5000 square degrees. Here we restricted our consideration to distant galaxies at the same redshift, but for a real survey with sources distributed in redshift, photometric redshift estimates can be obtained using observations in multiple filters. Tomographic information using the auto- and cross-correlations between the cosmic shear in various redshift bins, will give additional leverage in distinguishing between models of dark energy.

ACKNOWLEDGMENTS

SC is supported by Lincoln College, Oxford. LJK is supported by the Royal Society. We are grateful to Antony Lewis for reading the manuscript and for providing many helpful suggestions.

[3] http://terapix.iap.fr
[4] http://www.darkenergysurvey.org

REFERENCES

Albrecht A. J., et al., 2006. astro-ph/0609591
Alimi J. M., et al., 2009, Mon. Not. Roy. Astron. Soc., 401, 775
Bartelmann M., Schneider P., 2001, Phys. Rept., 340, 291
Benabed K., Bernardeau F., 2001, Phys. Rev., D64, 083501
Bernardeau F., Colombi S., Gaztanaga E., Scoccimarro R., 2002, Phys. Rept., 367, 1
Brax P., Martin J., 1999, Phys. Lett., B468, 40
Caldwell R. R., Dave R., Steinhardt P. J., 1998, Phys. Rev. Lett., 80, 1582
Carroll S. M., 1998, Phys. Rev. Lett., 81, 3067
Casarini L., Maccio' A. V., Bonometto S. A., 2009, JCAP, 0903, 014
Copeland E. J., Liddle A. R., Wands D., 1998, Phys. Rev., D57, 4686
Copeland E. J., Sami M., Tsujikawa S., 2006, Int. J. Mod. Phys., D15, 1753
Crocce M., Scoccimarro R., 2006, Phys. Rev., D73, 063519
Dent J. B., Dutta S., Weiler T. J., 2008, Phys. Rev., D80, 023514
Dodelson S., 2003, Modern Cosmology. Academic Press
Dolag K., et al., 2004, Astron. Astrophys., 416, 853
Ferreira P. G., Joyce M., 1998, Phys. Rev., D58, 023503
Frieman J., Turner M., Huterer D., 2008, Ann. Rev. Astron. Astrophys., 46, 385
Frieman J. A., Hill C. T., Stebbins A., Waga I., 1995, Phys. Rev. Lett., 75, 2077
Gilmozzi R., Spyromilio J., 2007, The ESO Messenger, 127, 11
Goldhaber G., Perlmutter S., 1998, Phys. Rept., 307, 325
Huterer D., 2002, Phys. Rev., D65, 063001
Hwang J.-C., 1991, Astrophys. J., 375, 443
Hwang J.-c., Park C.-G., Lee J.-h., Noh H., 2009, Phys. Rev. Lett., 103, 151303
Jain B., Seljak U., 1997, Astrophys. J., 484, 560
Jennings E., Baugh C. M., Angulo R. E., Pascoli S., 2009. 0908.1394
Jennings E., Baugh C. M., Angulo R. E., Pascoli S., 2010a, arXiv. 1002.3255
Jennings E., Baugh C. M., Pascoli S., 2010b, arXiv. 1003.4282
Kaiser N., 1998, Astrophys. J., 498, 26
Kessler R., et al., 2009, Astrophys. J. Suppl., 185, 32
Klypin A., Maccio A. V., Mainini R., Bonometto S. A., 2003, Astrophys. J., 599, 31
Kodama H., Sasaki M., 1984, Progress of Theoretical Physics Supplement, 78, 1
Komatsu E., et al., 2009, Astrophys. J. Suppl., 180, 330
Kowalski M., et al., 2008, Astrophys. J., 686, 749
Liddle A. R., Parkinson D., Leach S. M., Mukherjee P., 2006, Phys. Rev., D74, 083512
Ma C.-P., Caldwell R. R., Bode P., Wang L.-M., 1999, Astrophys. J., 521, L1
Maio U., et al., 2006, Mon. Not. Roy. Astron. Soc., 373, 869
Malik K. A., Wands D., 2004, Class. Quant. Grav., 21, L65
Peacock J. A., Dodds S. J., 1994, Mon. Not. Roy. Astron. Soc., 267, 1020
Peacock J. A., et al., 2006. astro-ph/0610906
Ratra B., Peebles P. J. E., 1988, Phys. Rev., D37, 3406
Refregier A., et al., 2004, Astron. J., 127, 3102
Riess A. G., et al., 1998, Astrophys. J., 116, 1009
Rudd D. H., Zentner A. R., Kravtsov A. V., 2008, Astrophys. J., 672, 19
Sapone D., Kunz M., 2009, Phys. Rev., D80, 083519
Smith R. E., et al., 2003, Mon. Not. Roy. Astron. Soc., 341, 1311
Solevi P., et al., 2006, Mon. Not. Roy. Astron. Soc., 366, 1346
Spergel D. N., et al., 2007, Astrophys. J. Suppl., 170, 377
Tyson J. A., 2002, Proc. SPIE Int. Soc. Opt. Eng., 4836, 10
Wetterich C., 1988, Nucl. Phys. B, 302, 668
White 1 M. J., 2004, Astropart. Phys., 22, 211
Wittman D. M., Tyson J. A., Kirkman D., Dell'Antonio I., Bernstein G., 2000, Nature, 405, 143